



COGNITIVE NEUROSCIENCE

Alpha-frequency feedback to early visual cortex orchestrates coherent naturalistic vision

Lixiang Chen^{1*}, Radoslaw M. Cichy^{1†}, Daniel Kaiser^{2,3*†}

During naturalistic vision, the brain generates coherent percepts by integrating sensory inputs scattered across the visual field. Here, we asked whether this integration process is mediated by rhythmic cortical feedback. In electroencephalography (EEG) and functional magnetic resonance imaging (fMRI) experiments, we experimentally manipulated integrative processing by changing the spatiotemporal coherence of naturalistic videos presented across visual hemifields. Our EEG data revealed that information about incoherent videos is coded in feedforward-related gamma activity while information about coherent videos is coded in feedback-related alpha activity, indicating that integration is indeed mediated by rhythmic activity. Our fMRI data identified scene-selective cortex and human middle temporal complex (hMT) as likely sources of this feedback. Analytically combining our EEG and fMRI data further revealed that feedback-related representations in the alpha band shape the earliest stages of visual processing in cortex. Together, our findings indicate that the construction of coherent visual experiences relies on cortical feedback rhythms that fully traverse the visual hierarchy.

Copyright © 2023 The Authors, some rights reserved; exclusive licensee American Association for the Advancement of Science. No claim to original U.S. Government Works. Distributed under a Creative Commons Attribution NonCommercial License 4.0 (CC BY-NC).

INTRODUCTION

We consciously experience our visual surroundings as a coherent whole that is phenomenally unified across space (1, 2). In our visual system, however, inputs are initially transformed into a spatially fragmented mosaic of local signals that lack integration. How does the brain integrate this fragmented information across the subsequent visual processing cascade to mediate unified perception?

Classic hierarchical theories of vision posit that integration is solved during feedforward processing (3, 4). On this view, integration is hard wired into the visual system: Local representations of specific features are integrated into more global representations of meaningful visual contents through hierarchical convergence over features distributed across visual space.

More recent theories instead posit that visual integration is achieved through complex interactions between feedforward information flow and dynamic top-down feedback (5–7). On this view, feedback information flow from downstream adaptively guides the integration of visual information in upstream regions. Such a conceptualization is anatomically plausible, as well as behaviorally adaptive, as higher-order regions can flexibly adjust current whether or not stimuli are integrated through the visual system's abundant top-down connections (8–10).

However, the proposed interactions between feedforward and feedback information pose a critical challenge: Feedforward and feedback information needs to be multiplexed across the visual hierarchy to avoid unwanted interferences through spurious interactions of these signals. Previous studies propose that neural systems meet this challenge by routing feedforward and feedback information in different neural frequency channels: High-frequency gamma (31 to 70 Hz) rhythms may mediate feedforward propagation,

whereas low-frequency alpha (8 to 12 Hz) and beta (13 to 30 Hz) rhythms carry predictive feedback to upstream areas (11–14).

Here, we set out to test the hypothesis that rhythmic coding acts as a mechanism mediating coherent visual perception. We used a novel experimental paradigm that manipulated the degree to which stimuli could be integrated across space through the spatiotemporal coherence of naturalistic videos shown in the two visual hemifields. Combining electroencephalography (EEG) and functional magnetic resonance imaging (fMRI) measurements, we show that when inputs are integrated into a coherent percept, cortical alpha dynamics carry stimulus-specific feedback from high-level visual cortex to early visual cortex. Our results show that spatial integration of naturalistic visual inputs is mediated by feedback dynamics that traverse the visual hierarchy in low-frequency alpha rhythms.

RESULTS

We experimentally mimicked the spatially distributed nature of naturalistic inputs by presenting eight 3-s naturalistic videos (Fig. 1A) through two circular apertures right and left of fixation (diameter, 6° visual angle; minimal distance to fixation, 2.64°). To assess spatial integration in a controlled way, we varied how the videos were presented through these apertures (Fig. 1B): In the right- or left-only condition, the video was shown only through one of the apertures, providing a baseline for processing inputs from one hemifield, without the need for spatial integration across hemifields. In the coherent condition, the same original video was shown through both apertures. Here, the input had the spatiotemporal statistics of a unified scene expected in the real world and could thus be readily integrated into a coherent unitary percept. In the incoherent condition, by contrast, the videos shown through the two apertures stemmed from two different videos (see fig. S1). Here, the input did not have the spatiotemporal real-world statistics of a unified scene and thus could not be readily integrated. Contrasting brain activity for the coherent and incoherent condition thus reveals

¹Department of Education and Psychology, Freie Universität Berlin, Berlin 14195, Germany. ²Mathematical Institute, Department of Mathematics and Computer Science, Physics, Geography, Justus-Liebig-Universität Gießen, Gießen 35392, Germany. ³Center for Mind, Brain and Behavior (CMBB), Philipps-Universität Marburg and Justus-Liebig-Universität Gießen, Marburg 35032, Germany. *Corresponding author. Email: lixiang.chen@fu-berlin.de (L.C.); danielkaiser.net@gmail.com (D.K.).

†These authors contributed equally to this work.

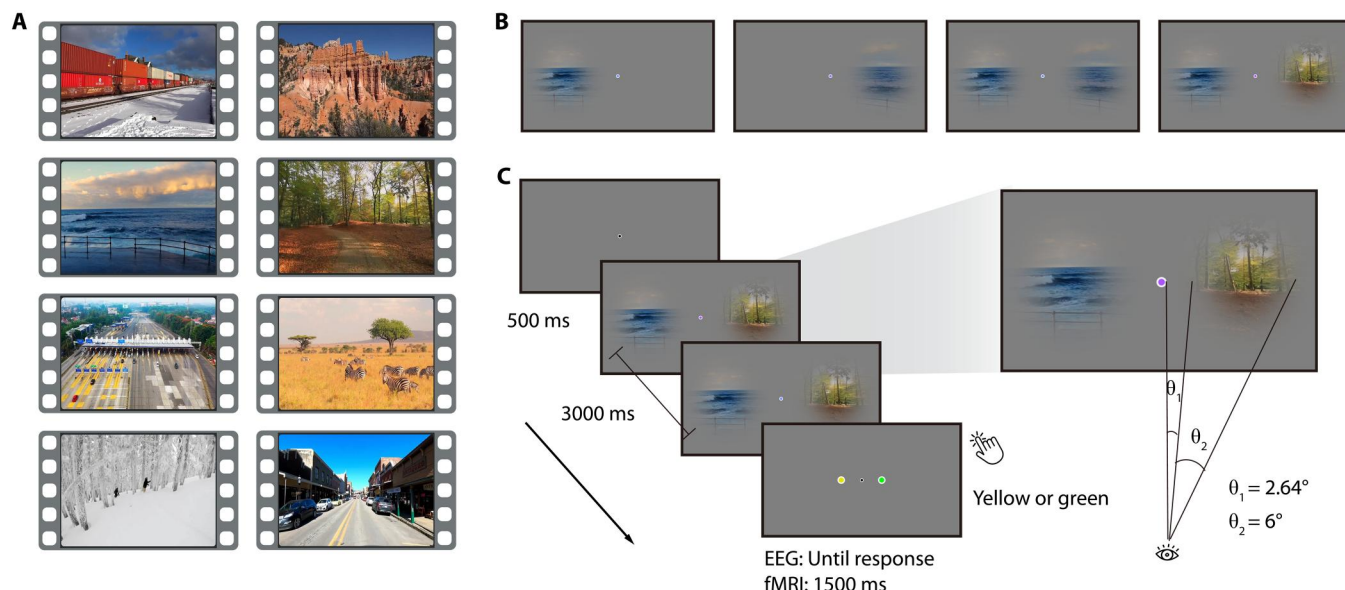


Fig. 1. Stimuli and experimental design. (A) Snapshots from the eight videos used. (B) In the experiment, videos were either presented through one aperture in the right or left visual field or through both apertures in a coherent or incoherent way. (C) During the video presentation, the color of the fixation dot changed periodically (every 200 ms). Participants reported whether a green or yellow fixation dot was included in the sequence.

neural signatures of spatial integration into unified percepts across visual space.

Participants viewed the video stimuli in separate EEG ($n = 48$) and fMRI ($n = 36$) recording sessions. Participants performed an unrelated central task (Fig. 1C) to ensure fixation and to allow us to probe integration processes in the absence of explicit task demands.

Harnessing the complementary frequency resolution and spatial resolution of our EEG and fMRI recordings, we then delineated how inputs that either can or cannot be integrated into a coherent percept are represented in rhythmic neural activity and regional activity across the visual hierarchy. Specifically, we decoded between the eight different video stimuli in each of the four conditions from frequency-resolved EEG sensor patterns (15, 16) and from spatially resolved fMRI multivoxel patterns (17).

Rhythmic brain dynamics mediate integration across visual space

Our first key analysis determined how the feedforward and feedback information flows involved in the processing and integrating visual information across space are multiplexed in rhythmic codes. We hypothesized that conditions not affording integration lead to neural coding in feedforward-related gamma activity (11, 14), whereas conditions that allow for spatiotemporal integration lead to coding in feedback-related alpha/beta activity (11, 14).

To test this hypothesis, we decoded the video stimuli from spectrally resolved EEG signals, aggregated within the alpha, beta, and gamma frequency bands, during the whole stimulus duration (Fig. 2A; see Materials and Methods for details). Our findings supported our hypothesis. We observed that incoherent video stimuli, as well as single video stimuli, were decodable only from the gamma frequency band [all $t(47) > 3.41$, $P < 0.001$; Fig. 2, B and C]. By stark contrast, coherent video stimuli were decodable only from the alpha-frequency band [$t(47) = 5.43$, $P < 0.001$; Fig. 2C]. Comparing

the pattern of decoding performance across frequency bands revealed that incoherent video stimuli were better decodable than coherent stimuli from gamma responses [$t(47) = 3.04$, $P = 0.004$] and coherent stimuli were better decoded than incoherent stimuli from alpha responses [$t(47) = 2.32$, $P = 0.025$; interaction: $F(2, 94) = 7.47$, $P < 0.001$; Fig. 2C]. The observed effects also held when analyzing the data continuously across frequency space rather than aggregated in predefined frequency bands (see fig. S2) and were not found trivially in the evoked broadband responses (see fig. S3). We also analyzed the theta (4 to 7 Hz) and high-gamma bands (71 to 100 Hz) using the decoding analysis. For the theta band, we did not find any significant decoding (see figs. S2 and S4). The results from the high-gamma band were highly similar to the results obtained for the lower-gamma frequency range (see figs. S2 and S4). In addition, we conducted both univariate and decoding analyses on time- and frequency-resolved responses, but neither of these analyses revealed any differences between the coherent and incoherent conditions (see fig. S5), indicating a lack of statistical power for resolving the data both in time and frequency. Together, our results demonstrate the multiplexing of visual information in rhythmic information flows. When no integration across hemifields was required, visual feedforward activity is carried by gamma rhythms. When spatiotemporally coherent inputs allow for integration, integration-related feedback activity is carried by alpha rhythms.

The observation of a frequency-specific channel for feedback information underlying spatial integration immediately poses two questions: (i) Where does this feedback originate from? and (ii) Where is this feedback heading? We used fMRI recordings to answer these two questions in turn.

Scene-selective cortex is the source of integration-related feedback

To reveal the source of the feedback, we evaluated how representations across visual cortex differ between stimuli that can or cannot

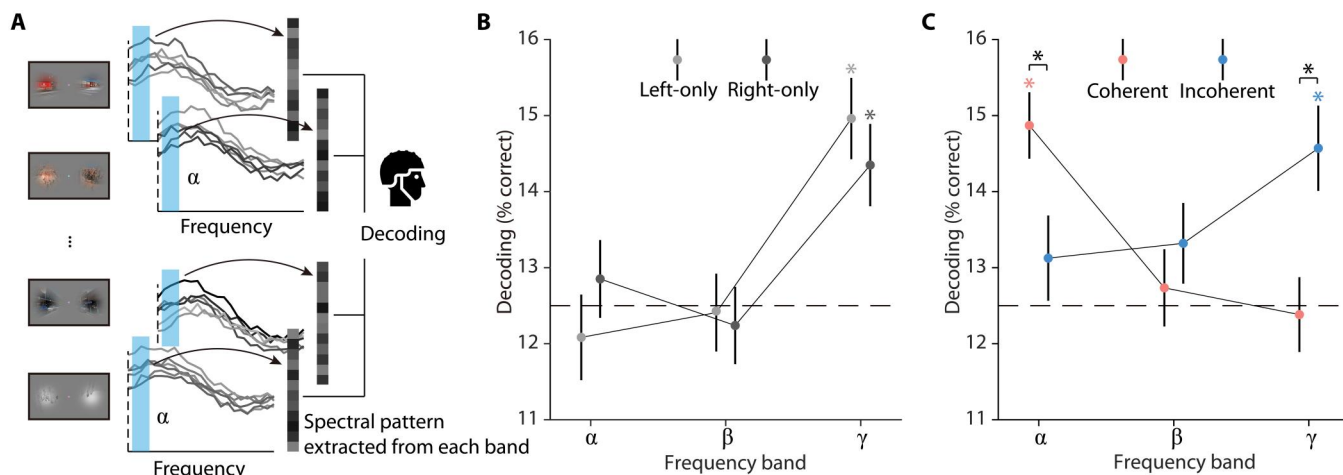


Fig. 2. EEG decoding analysis. (A) Frequency-resolved EEG decoding analysis. In each condition, we used eight-way decoding to classify the video stimuli from patterns of spectral EEG power across electrodes, separately for each frequency band (alpha, beta, and gamma). (B and C) Results of EEG frequency-resolved decoding analysis. The incoherent and single video stimuli were decodable from gamma responses, whereas the coherent stimuli were decodable from alpha responses, suggesting a switch from dominant feedforward processing to the recruitment of cortical feedback. Error bars represent SEs. * $P < 0.05$ (FDR-corrected).

be integrated across space (Fig. 3A). We reasoned that regions capable of exerting integration-related feedback should show stronger representations of spatiotemporally coherent inputs that can be integrated, compared to incoherent inputs that do not. Scene-selective areas in visual cortex are a strong contender for the source of this feedback, as they have been previously linked to the spatial integration of coherent scene information (18, 19).

To test this assertion, we decoded the video stimuli from multi-voxel patterns in a set of three early visual cortex regions (V1, V2, and V3), one motion-selective region [human middle temporal complex (hMT)/V5], and three scene-selective regions [the occipital place area (OPA), the medial place area (MPA), and the parahippocampal place area (PPA)].

In a first step, we decoded between the single video stimuli and found information in early visual cortex (V1, V2, and V3) and scene-selective cortex (OPA, MPA, and PPA) only when video stimuli were shown in the hemifield contralateral to the region investigated [all $t(35) > 3.75$, $P < 0.001$; Fig. 3B]. This implies that any stronger decoding for coherent, compared to incoherent, video stimuli can only be driven by the interaction of ipsilateral and contralateral inputs, rather than by the ipsilateral input alone. On this interpretative backdrop, we next decoded coherent and incoherent video stimuli. Both were decodable in each of the seven regions [all $t(35) > 4.43$, $P < 0.001$; Fig. 3C]. Critically, coherent video stimuli were only better decoded than incoherent stimuli in the MPA [$t(35) = 3.61$, $P < 0.001$; Fig. 3C] and PPA [$t(35) = 3.32$, $P = 0.002$; Fig. 3C]. A similar trend was found in hMT [$t(35) = 1.73$, $P = 0.092$; Fig. 3C]. In hMT, MPA, and PPA, coherent video stimuli were also better decoded than contralateral single video stimuli [all $t(35) > 2.99$, $P < 0.005$]. Similar results were found in the whole-brain searchlight-decoding analysis. We found significant decoding for single video stimuli across the visual cortex in the contralateral hemisphere (see fig. S6) as well as significant decoding across the visual cortex for both coherent (Fig. 3D) and incoherent stimuli (Fig. 3E). The differences between coherent and incoherent conditions were only found in locations overlapping—or close to—scene-selective cortex and hMT (Fig. 3F). Given the involvement

of motion-selective hMT in integrating visual information, we also tested whether differences in motion coherence (operationalized as motion energy and motion direction) contribute to the integration effects observed here. When assessing differences between videos with high and low motion coherence across hemifields, however, we did not find qualitatively similar effects to our main analyses (see fig. S7), suggesting that motion coherence is not the main driver of the integration effects.

Together, these results show that scene-selective cortex and hMT aggregate spatiotemporally coherent information across hemifields, suggesting these regions as likely generators of feedback signals guiding visual integration.

Integration-related feedback traverses the visual hierarchy

Last, we determined where the feedback-related alpha rhythms are localized in brain space. We were particularly interested in whether integration-related feedback traverses the visual hierarchy up to the earliest stages of visual processing (20, 21). To investigate this, we performed an EEG/fMRI fusion analysis (22, 23) that directly links spectral representations in the EEG with spatial representations in the fMRI. To link representations across modalities, we first computed representational similarities between all video stimuli using pairwise decoding analyses and then correlated the similarities obtained from EEG alpha responses and fMRI activations across the seven visual regions (Fig. 4A). Here, we focused on the crucial comparison of regional representations (fMRI) and alpha-frequency representations (EEG) between the coherent and the incoherent conditions. Our fMRI decoding analyses for the single video stimuli demonstrate that V1 only receives sensory information from the contralateral visual field. As feedforward inputs from the contralateral visual field are identical across both conditions, any stronger correspondence between regional representations and alpha-frequency representations in the coherent condition can unequivocally be attributed to feedback from higher-order systems, which have access to both ipsi- and contralateral input. We found that representations in the alpha band were more strongly related to representations in the coherent condition

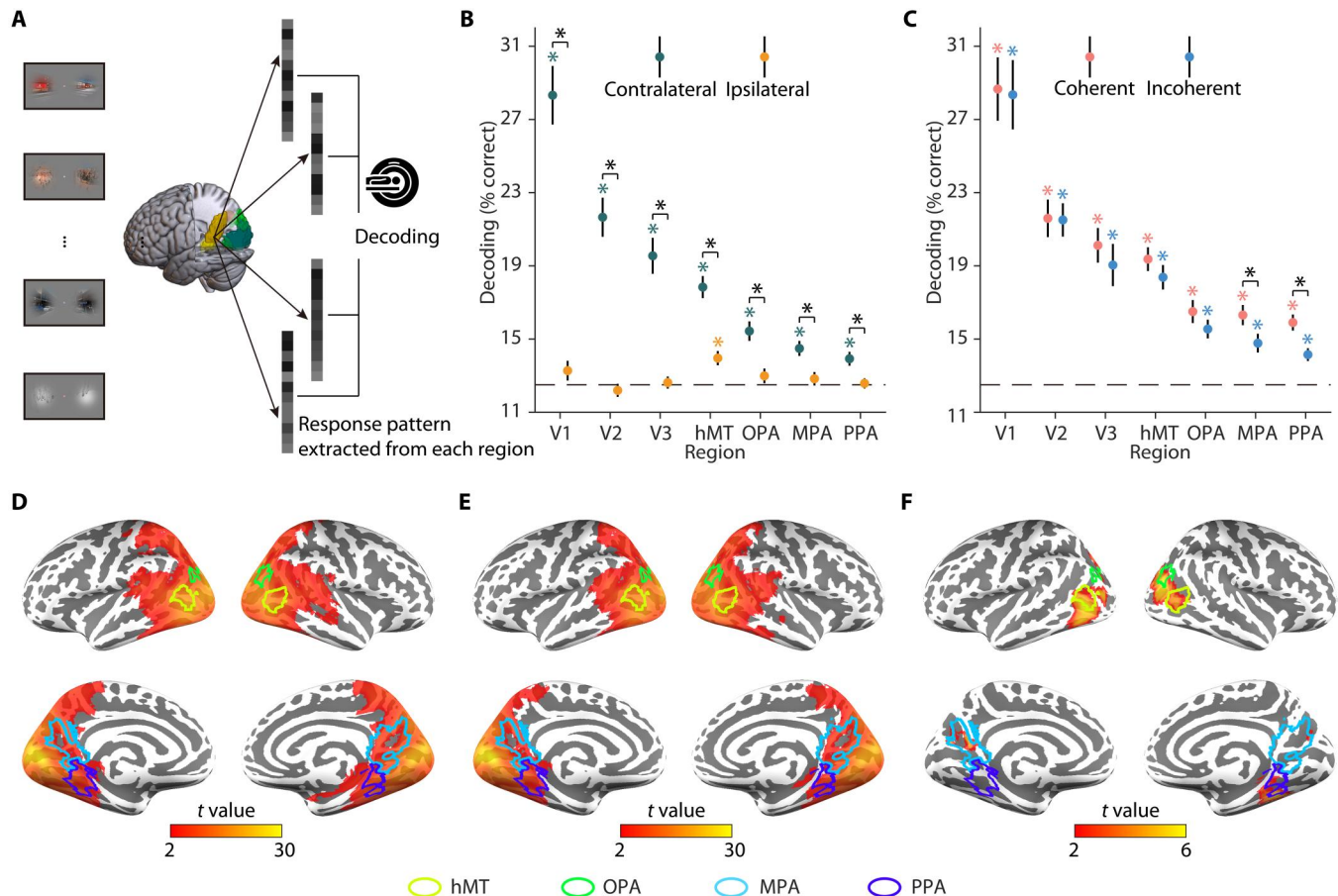
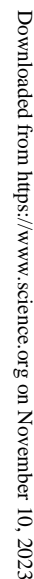


Fig. 3. fMRI decoding analysis. (A) fMRI decoding analysis in regions of interest (ROIs). In each condition, we used eight-way decoding to classify the video stimuli on response patterns in each ROI (V1, V2, V3, hMT, OPA, MPA, and PPA). (B) Results of fMRI ROI decoding analysis for the right- and left-only conditions. Single video stimuli were decodable in regions contralateral to the stimulation. In the ipsilateral hemisphere, they were only decodable in hMT but not in early visual cortex (V1, V2, and V3) and scene-selective cortex (OPA, MPA, and PPA). (C) Results of fMRI ROI decoding analysis for the coherent and incoherent conditions. Video stimuli were decodable in both conditions in each of the seven regions. Coherent stimuli were decoded better than incoherent stimuli in scene-selective cortex (MPA and PPA). (D) Results of fMRI searchlight decoding analysis for the coherent condition. Coherent stimuli were decodable across visual cortex. (E) Results of fMRI searchlight decoding analysis for the incoherent condition. Incoherent stimuli were decodable across visual cortex. (F) Significant differences between coherent and incoherent conditions in fMRI searchlight decoding analysis. Significant differences between the coherent and incoherent conditions were observed in locations overlapping—or close to—scene-selective cortex and hMT. Together, the results suggested that scene-selective cortex and hMT integrate dynamic information across visual hemifields. Error bars represent SEs. * $P < 0.05$ (FDR-corrected).

than in the incoherent condition in V1 [$t(35) = 3.37$, $P = 0.001$; Fig. 4B]. A similar trend emerged in V2 [$t(35) = 2.32$, $P_{\text{uncorrected}} = 0.025$; Fig. 4B] and V3 [$t(35) = 2.15$, $P_{\text{uncorrected}} = 0.036$; Fig. 4B] but not in hMT [$t(35) = -0.28$, $P = 0.783$; Fig. 4B] and scene-selective cortex [OPA: $t(35) = 0.94$, $P = 0.351$; MPA: $t(35) = 0.005$, $P = 0.996$; PPA: $t(35) = -1.64$, $P = 0.108$; Fig. 4B]. The correspondence between alpha-band representations in the EEG and activity in early visual cortex persisted after we controlled for motion coherence in the fusion analysis (see fig. S8), suggesting that the effect was not solely attributable to coherent patterns of motion. By contrast, no such correspondences were found between beta/gamma EEG responses and regional fMRI activations (see fig. S9). The results of the fusion analysis show that when inputs are spatiotemporally coherent and can be integrated into a unified percept, feedback-related alpha rhythms are found at the earliest stages of visual processing in cortex.

DISCUSSION

Our findings demonstrate that the spatial integration of naturalistic inputs integral to mediating coherent perception is achieved by cortical feedback: Only when spatiotemporally coherent inputs can be integrated into a coherent whole, stimulus-specific information was coded in feedback-related alpha activity. We further show that scene-selective cortex and hMT interactively process information across visual space, highlighting them as likely sources of integration-related feedback. Last, we reveal that integration-related alpha dynamics are linked to representations in early visual cortex, indicating that integration is accompanied by feedback that traverses the whole cortical visual hierarchy from top to bottom. Together, our results promote an active conceptualization of the visual system, where concurrent feedforward and feedback information flows are critical for establishing coherent naturalistic vision.



Our results inform theories about the functional role of alpha rhythms in cortex. Alpha is often considered an idling rhythm (42, 43), a neural correlate of active suppression (44–46), or a correlate of working memory maintenance (47, 48). More recently, alpha rhythms were associated with an active role in cortical feedback processing (12, 14, 49, 50). Our results highlight that alpha dynamics not only modulate feedforward processing but also encode stimulus-specific information. Our findings thus invite a different conceptualization of alpha dynamics, where alpha rhythms are critically involved in routing feedback-related information across the visual cortical hierarchy (15, 16, 51, 52). An important remaining question is whether the feedback itself traverses in alpha rhythms or whether the feedback initiates upstream representations that

themselves fluctuate in alpha rhythms (53, 54). The absence of a correspondence of alpha-band representations and regional activity in scene-selective cortex may suggest that it is not the feedback itself that is rhythmic, but alpha dynamics in scene-selective cortex may also be weaker—or to some extent initiated for both coherent and incoherent stimuli. More studies are needed to dissociate between the rhythmic nature of cortical feedback and the representations it instills in early visual cortex.

The increased involvement of alpha rhythms in coding the coherent visual stimuli was accompanied by an absence of concurrent representations in the gamma band. A potential reason for the absence of decoding from feedforward-related gamma activity in the coherent condition is that feedforward representations were efficiently suppressed by accurate top-down predictions (5). In our experiment, the video stimuli were presented for a relatively long time, without many rapid or unexpected visual events, potentially silencing feedforward propagation in the gamma range. We also did not find a correspondence between gamma dynamics and regional fMRI activity. Despite a general difficulty in linking high-frequency EEG activity and fMRI signals, another reason may be that, unlike the alpha dynamics, the gamma dynamics were relatively broad-band and did not reflect a distinct neural rhythm (see fig. S2).

Our findings can be linked to theories of predictive processing that view neural information processing as a dynamic exchange of sensory feedforward signals and predictions stemming from higher-order areas of cortex (5, 6, 51). On this view, feedback signals arising during stimulus integration are conceptualized as predictions about sensory input derived from spatially and temporally coherent contralateral input. In our paradigm, feedback signals can be conceptualized as predictions for the contralateral input generated from the spatiotemporally coherent ipsilateral input. A challenge for predictive coding theories is that it requires a strict separation of the feedforward sensory input and the predictive feedback. Our results indicate a compelling solution through multiplexing of feedforward and feedback information in dedicated frequency-specific channels (11, 13, 14, 49) in human cortex. It will be interesting to see whether similar frequency-specific correlates of predictive processing are unveiled in other brain systems in the future.

Our findings further pave the way toward researching integration processes under various task demands. In our experiments, we engaged participants in an unrelated fixation task, capitalizing on automatically triggered integration processes for spatiotemporally coherent stimuli. Such automatic integration is well in line with phenomenological experience: The coherent video stimuli, but not the incoherent stimuli, strongly appear as coherent visual events that happen behind an occlude. Future studies should investigate how integration effects vary when participants are required to engage with the stimuli that need to be integrated. It will be particularly interesting to see whether tasks that require more global or local analysis are related to different degrees of integration and different rhythmic codes in the brain. These future studies could also set out to determine the critical features that enable integration and what is integrated. As our incoherent stimuli were designed to be incoherent along many different dimensions (e.g., low- and mid-level visual features, categorical content, and motion patterns), a comprehensive mapping of how these dimensions independently contribute to integration is needed. Future studies could thereby delineate how integration phenomenologically depends on the coherence of these candidate visual features.

More generally, our results have general implications for understanding and modeling feedforward and feedback information flows in neural systems. Processes like stimulus integration that are classically conceptualized as solvable in pure feedforward cascades may be more dynamic than previously thought. Discoveries like ours arbitrate between competing theories that either stress the power of feedforward hierarchies (3, 4) or emphasize the critical role of feedback processes (5, 6). They further motivate approaches to computational modeling that capture the visual system's abundant feedback connectivity (55, 56).

Together, our results reveal feedback in the alpha-frequency range across the visual hierarchy as a key mechanism for integrating spatiotemporally coherent information in naturalistic vision. This strongly supports an active conceptualization of the visual system, where top-down projections are critical for the construction of coherent and unified visual percepts from fragmented sensory information.

MATERIALS AND METHODS

Participants

Forty-eight healthy adults (gender: 12 males/36 females, age: 21.1 ± 3.8 years) participated in the EEG experiment, and another 36 (gender: 17 males/19 females, age: 27.3 ± 2.5 years) participated in the fMRI experiment. Sample size resulted from convenience sampling, with the goal of exceeding $n = 34$ in both experiments (i.e., exceeding 80% power for detecting a medium effect size of $d = 0.5$ in a two-sided t test). All participants had normal or corrected-to-normal vision and had no history of neurological/psychiatric disorders. They all signed informed consent before the experiment, and they were compensated for their time with partial course credit or cash. The EEG protocol was approved by the ethical committee of the Department of Psychology at the University of York, and the fMRI protocol was approved by the ethical committee of the Department of Psychology at Freie Universität Berlin. All experimental protocols were in accordance with the Declaration of Helsinki.

Stimuli and design

The stimuli and design were identical for the EEG and fMRI experiments unless stated otherwise. Eight short video clips (3 s each; Fig. 1A) depicting everyday situations (e.g., a train driving past the observer; a view of red mountains; a view of waves crashing on the coast; first-person perspective of walking along a forest path; an aerial view of a motorway toll station; a group of zebras grazing on a prairie; first-person perspective of skiing in the forest; and first-person perspective of walking along a street) were used in the experiments. During the experiment, these original videos were presented on the screen through circular apertures right and left of central fixation. We manipulated four experimental conditions (right-only, left-only, coherent, and incoherent) by presenting the original videos in different ways (Fig. 1B). In the right- or left-only condition, we presented the videos through right or left aperture only. We also showed two matching segments from the same video in the coherent condition, while we showed segments from two different videos in the incoherent condition, through both apertures. In the incoherent condition, the eight original videos were yoked into eight fixed pairs (see fig. S1), and each video was always only shown with its paired video. Thus, there

were a total of 32 unique video stimuli (8 for each condition). The diameter of each aperture was 6° visual angle, and the shortest distance between the stimulation and central fixation was 2.64° visual angle. The borders of the apertures were slightly smoothed. The central fixation dot subtended 0.44° visual angle. We selected our videos to be diverse in content (e.g., natural versus manmade) and motion (e.g., natural versus camera motion). This was done to maximize the contrast between the coherent and incoherent video stimuli. For assessing motion, we quantified the motion energy for each video stimulus using Motion Energy Analysis software (<https://psync.ch/mea/>). We did not find any significant between-condition differences [comparison on the means of motion energy: right- versus left-only, $t(7) = 0.36$, $P = 0.728$, coherent versus incoherent, $t(7) = 0.03$, $P = 0.976$; comparison on the SDs of motion energy: right- versus left-only, $t(7) = 1.08$, $P = 0.316$, coherent versus incoherent, $t(7) = 1.13$, $P = 0.294$]. Although this suggests that there was no difference in overall motion between conditions, there are many other candidates for critical differences between conditions, which will have to be evaluated in future studies.

The experiments were controlled through MATLAB and the Psychophysics Toolbox (57, 58). In each trial, a fixation dot was first shown for 500 ms, after which a unique video stimulus was displayed for 3000 ms. During the video stimulus playback, the color of the fixation changed periodically (every 200 ms) and turned either green or yellow at a single random point in the sequence (but never the first or last point). After every trial, a response screen prompted participants to report whether a green or yellow fixation dot was included in the sequence. Participants were instructed to keep central fixation during the sequence so they would be able to solve this task accurately. In both experiments, participants performed the color discrimination with high accuracy (EEG: $93.28 \pm 1.65\%$ correct; fMRI: $91.44 \pm 1.37\%$ correct), indicating that they indeed focused their attention on the central task. There were no significant differences in behavioral accuracy and response time (RT) between the coherent and incoherent conditions in both the EEG and fMRI experiments [accuracy-EEG, $t(47) = 1.07$, $P = 0.29$; accuracy-fMRI, $t(35) = 0.20$, $P = 0.85$; RT-fMRI, $t(35) = 0.41$, $P = 0.69$]. Note that RTs were not recorded in the EEG experiment. The mean accuracy and RT for each condition in both experiments are listed in table S1. In the EEG experiment, the next trial started once the participant's response was received. In the fMRI experiment, the response screen stayed on the screen for 1500 ms, irrespective of participants' RT. An example trial is shown in Fig. 1C.

In the EEG experiment, each of the 32 unique stimuli was presented 20 times, resulting in a total of 640 trials, which were presented in random order. In the fMRI experiment, participants performed 10 identical runs. In each run, each unique stimulus was presented twice, in random order. Across the 10 runs, this also resulted in a total of 640 trials. The extensive repetition of the incoherent combinations may lead to some learning of the inconsistent stimuli in our experiment (59). However, such learning would, if anything, lead to an underestimation of the effects: Learning of the incoherent combination would ultimately also lead to an integration of the incoherent stimuli and thus create similar—albeit weaker—neural signatures of integration as found in the coherent condition.

To make sure that our intuition about the coherence of video stimuli in the coherent and incoherent conditions is valid, we

conducted an additional behavioral experiment on 10 participants (gender: 4 males/6 females, age: 24.8 ± 2.5 years). In the experiment, we presented each of the coherent and incoherent video stimuli once. After each trial, we asked the participants to rate the degree of unified perception of the stimulus on a 1 to 5 scale. We found that the rating of coherent stimuli was higher than the rating of incoherent stimuli (mean ratings for coherent stimuli: 4.1 to 4.6, mean ratings for incoherent stimuli: 1.2 to 1.6; $t(9) = 36.66$, $P < 0.001$), showing that the coherent stimuli were indeed rated as more coherent than the incoherent ones.

To assess the general fixation stability for our paradigm, we collected additional eye-tracking data from six new participants (see fig. S10 for details). We calculated the mean and SD of the horizontal and vertical eye movement across time (0 to 3 s) in each trial and then averaged the mean and SD values across trials separately for each condition. For all participants, we found means of eye movement lower than 0.3° , and SDs of eye movement lower than 0.2° , indicating stable central fixation (see fig. S10A). In addition, participants did not disengage from fixating after the target color was presented (see fig. S10B).

EEG recording and preprocessing

EEG signals were recorded using an ANT waveguard 64-channel system and a TSMi REFA amplifier, with a sample rate of 1000 Hz. The electrodes were arranged according to the standard 10-10 system. EEG data preprocessing was performed using FieldTrip (60). The data were first band-stop filtered to remove 50-Hz line noise and then band-pass filtered between 1 and 100 Hz. The filtered data were epoched from -500 to 4000 ms relative to the onset of the stimulus, re-referenced to the average over the entire head, downsampled to 250 Hz, and baseline corrected by subtracting the mean prestimulus signal for each trial. After that, noisy channels and trials were removed by visual inspection, and the removed channels (2.71 ± 0.19 channels) were interpolated by the mean signals of their neighboring channels. Blinks and eye movement artifacts were removed using independent component analysis and visual inspection of the resulting components.

EEG power spectrum analysis

Spectral analysis was performed using FieldTrip. Power spectra were estimated between 8 and 70 Hz (from alpha to gamma range), from 0 to 3000 ms (i.e., the period of stimulus presentation) on the preprocessed EEG data, separately for each trial and each channel. A single taper with a Hanning window was used for the alpha band (8 to 12 Hz, in steps of 1 Hz) and the beta band (13 to 30 Hz, in steps of 2 Hz), and the discrete prolate spheroidal sequences multitaper method with ± 8 Hz smoothing was used for the gamma band (31 to 70 Hz, in steps of 2 Hz).

EEG decoding analysis

To investigate whether the dynamic integration of information across the visual field is mediated by oscillatory activity, we performed multivariate decoding analysis using CoSMoMvPA (61) and the Library for Support Vector Machines (LIBSVM) (62). In this analysis, we decoded between the eight video stimuli using patterns of spectral power across channels, separately for each frequency band (alpha, beta, and gamma) and each condition. Specifically, for each frequency band, we extracted the power of the frequencies included in that band (e.g., 8 to 12 Hz for the alpha band) across all

channels from the power spectra and then used the resulting patterns across channels and frequencies to classify the eight video stimuli in each condition. For all classifications, we used linear support vector machine (SVM) classifiers to discriminate the eight stimuli in a 10-fold cross-validation scheme. For each classification, the data were allocated to 10 folds randomly, and then an SVM classifier was trained on data from 9 folds and tested on data from the left-out fold. The classification was done repeatedly until every fold was left out once, and accuracies were averaged across these repetitions. The amount of data in the training set was always balanced across stimuli. For each classification, a maximum of 144 trials (some trials were removed during preprocessing) were included in the training set (18 trials for each stimulus) and 16 trials were used for testing (2 trials for each stimulus). Before classification, principal components analysis (PCA) was applied to reduce the dimensionality of the data (63). Specifically, for each classification, PCA was performed on the training data, and the PCA solution was projected onto the testing data. For each PCA, we selected the set of components that explained 99% of the variance of the training data. As a result, we obtained decoding accuracies for each frequency band and each condition, which indicated how well the video stimuli were represented in frequency-specific neural activity. We first used a one-sample *t* test to investigate whether the video stimuli could be decoded in each condition and each frequency band. We also performed a 2-condition (coherent and incoherent) \times 3-frequency (alpha, beta, and gamma) two-way analysis of variance (ANOVA) and post hoc paired *t* tests [false discovery rate (FDR)—corrected across frequencies; $P_{\text{corrected}} < 0.05$] to compare the decoding differences between coherent and incoherent conditions separately for each frequency band. The comparisons of right- and left-only conditions were conducted using the same approaches. To track where the effects appeared across a continuous frequency space, we also decoded between the eight stimuli at each frequency from 8 to 70 Hz using a sliding window approach with a five-frequency resolution (see fig. S2).

fMRI recording and processing

MRI data were acquired using a 3T Siemens Prisma scanner (Siemens, Erlangen, Germany) equipped with a 64-channel head coil. T2*-weighted BOLD images were obtained using a multiband gradient-echo echo-planar imaging (EPI) sequence with the following parameters: multiband factor = 3, repetition time (TR) = 1500 ms, echo time (TE) = 33 ms, field of view = 204 mm by 204 mm, voxel size = 2.5 mm by 2.5 mm by 2.5 mm, 70° flip angle, 57 slices, and 10% interslice gap. Field maps were also obtained with a double-echo gradient echo field map sequence (TR = 545 ms, TE1/TE2 = 4.92 ms/7.38 ms) to correct for distortion in EPI. In addition, a high-resolution 3D T1-weighted image was collected for each participant (magnetization-prepared rapid gradient-echo, TR = 1900 ms, TE = 2.52 ms, TI = 900 ms, 256 \times 256 matrix, 1-mm by 1-mm by 1-mm voxel, 176 slices).

MRI data were preprocessed using MATLAB and SPM12 (www.fil.ion.ucl.ac.uk/spm/). Functional data were first corrected for geometric distortion with the SPM FieldMap toolbox (64) and realigned for motion correction. In addition, individual participants' structural images were coregistered to the mean realigned functional image, and transformation parameters to Montreal Neurological Institute (MNI) standard space (as well as inverse transformation parameters) were estimated.

The GLMsingle Toolbox (65) was used to estimate the fMRI responses to the stimulus in each trial based on realigned fMRI data. To improve the accuracy of trialwise beta estimations, a three-stage procedure was used, including identifying an optimal hemodynamic response function (HRF) for each voxel from a library of 20 HRFs, denoising data-driven nuisance components identified by cross-validated PCA, and applying fractional ridge regression to regularize the beta estimation on a single-voxel basis. The resulting single-trial betas were used for further decoding analyses.

fMRI regions of interest definition

fMRI analyses were focused on seven regions of interest (ROIs). We defined three scene-selective areas—OPA [also termed transverse occipital sulcus (66, 67)], MPA [also termed retrosplenial cortex (68, 69)], and PPA (70)—from a group functional atlas (71) and three early visual areas—V1, V2, and V3, as well as motion-selective hMT/V5—from a probabilistic functional atlas (72). All ROIs were defined in MNI space and separately for each hemisphere and then transformed into individual-participant space using the inverse normalization parameters estimated during preprocessing.

fMRI ROI decoding analysis

To investigate how the video stimuli were processed in different visual regions, we performed multivariate decoding analysis using CoSMoMVPA and LIBSVM. For each ROI, we used the beta values across all voxels included in the region to decode between the eight video stimuli, separately for each condition. Leave-one-run-out cross-validation and PCA were used to conduct SVM classifications. For each classification, there were 144 trials (18 for each stimulus) in the training set and 16 trials (2 for each stimulus) in the testing set. For each participant, we obtained a 4-condition \times 14-ROI (7 ROIs by two hemispheres) decoding matrix. Results were averaged across hemispheres, as we consistently found no significant interhemispheric differences (condition \times hemisphere and condition \times region \times hemisphere interaction effects) in a 2-condition (coherent and incoherent) \times 7-region (V1, V2, V3, hMT, OPA, MPA, and PPA) \times 2-hemisphere (left and right) three-way ANOVA test. We first tested whether the video stimuli were decodable in each condition and each region using one-sample *t* tests (FDR-corrected across regions; $P_{\text{corrected}} < 0.05$). To further investigate the integration effect, we used paired *t* tests to compare the decoding difference between coherent and incoherent conditions in different regions. For the right- and left-only conditions, we averaged the decoding results in a contralateral versus ipsilateral fashion (e.g., left stimulus, right brain region was averaged with right stimulus, left brain region to obtain the contralateral decoding performance).

fMRI searchlight decoding analysis

To further investigate the whole-brain representation of video stimuli, we performed searchlight decoding analyses using CoSMoMVPA and LIBSVM. The single-trial beta maps in the native space were first transformed into the MNI space using the normalization parameters estimated during preprocessing. For the searchlight analysis, we defined a sphere with a radius of five voxels around a given voxel and then used the beta values of the voxels within this sphere to classify the eight video stimuli in each condition. For the left- and right-only conditions, the decoding analysis was performed separately for each hemisphere. The decoding parameters were identical to the ROI-decoding analysis. The resulting

searchlight maps were subsequently smoothed with a Gaussian kernel (full width at half maximum = 6 mm). To investigate how well the video stimuli in each condition were represented across the whole brain, we used one-sample *t* tests to compare decoding accuracies against chance separately for each condition [Gaussian random field (GRF) correction, voxel-level $P < 0.005$, cluster-extent $P < 0.05$]. To investigate the integration effect in the whole brain, we used paired *t* tests to compare the differences in decoding accuracy between coherent and incoherent conditions and performed multiple comparisons correction within the voxels showing significant decoding for either coherent or incoherent stimuli (GRF correction, voxel-level $P < 0.005$, cluster-extent $P < 0.05$).

EEG-fMRI fusion with representational similarity analysis

To investigate the relationship between the frequency-specific effects obtained in the EEG and the spatial mapping obtained in the fMRI, we performed EEG-fMRI fusion analysis (22, 23). This analysis can be used to compare neural representations of stimuli as characterized by EEG and fMRI data to reveal how the representations correspond across brain space and spectral signatures. Specifically, we first calculated representational dissimilarity matrices (RDMs) using pairwise decoding analysis for EEG and fMRI data, respectively. For the EEG power spectra, in each frequency band, we decoded between each pair of eight video stimuli using the oscillatory power of the frequencies included in the frequency band, separately for each condition; for the fMRI data, in each ROI, we classified each pair of eight stimuli using the response patterns of the region, separately for each condition. Decoding parameters were otherwise identical to the eight-way decoding analyses (see above). In each condition, we obtained a participant-specific EEG RDM (8 stimuli \times 8 stimuli) in each frequency band and a participant-specific fMRI RDM (8 stimuli \times 8 stimuli) in each ROI. Next, we calculated the similarity between EEG and fMRI RDMs for each condition; this was done by correlating all lower off-diagonal entries between the EEG and fMRI RDMs (the diagonal was always left out). To increase the signal-to-noise ratio, we first averaged fMRI RDMs across participants and then calculated the Spearman correlation between the averaged fMRI RDM for each ROI with the participant-specific EEG RDM for each frequency. As a result, we obtained a 4-condition \times 3-frequency \times 14-ROI fusion matrix for each EEG participant. For the coherent and incoherent conditions, the results were averaged across hemispheres, as no condition \times hemisphere, no condition \times region \times hemisphere, and no condition \times frequency \times hemisphere interaction effects were found in a 2-condition (coherent and incoherent) \times 7-region (V1, V2, V3, hMT, OPA, MPA, and PPA) \times 2-hemisphere (left and right) \times 3-frequency (alpha, beta, and gamma) four-way ANOVA test. We first used one-sample *t* tests to test the fusion effect in each condition (FDR-corrected across regions; $P_{\text{corrected}} < 0.05$) and each frequency-region combination and then used a 2-condition \times 3-frequency \times 7-region three-way ANOVA to compare the frequency-region correspondence between coherent and incoherent conditions. As we found a significant condition \times frequency \times region interaction effect, we further performed a 2-condition \times 7-region ANOVA and paired *t* tests (FDR-corrected across regions; $P_{\text{corrected}} < 0.05$) to compare frequency-region correspondence between coherent and incoherent conditions separately for each frequency. For the right- and left-only conditions, we averaged the fusion results

across two conditions separately for contralateral and ipsilateral presentations and then compared contralateral and ipsilateral presentations using the same approaches we used for the comparisons of coherent and incoherent conditions (see fig. S9).

Supplementary Materials

This PDF file includes:

Figs. S1 to S10

Table S1

REFERENCES AND NOTES

1. N. Block, Consciousness, accessibility, and the mesh between psychology and neuroscience. *Behav. Brain Sci.* **30**, 481–499 (2007).
2. M. A. Cohen, D. C. Dennett, N. Kanwisher, What is the bandwidth of perceptual experience? *Trends Cogn. Sci.* **20**, 324–335 (2016).
3. M. Riesenhuber, T. Poggio, Hierarchical models of object recognition in cortex. *Nat. Neurosci.* **2**, 1019–1025 (1999).
4. J. J. DiCarlo, D. D. Cox, Untangling invariant object recognition. *Trends Cogn. Sci.* **11**, 333–341 (2007).
5. R. P. N. Rao, D. H. Ballard, Predictive coding in the visual cortex: A functional interpretation of some extra-classical receptive-field effects. *Nat. Neurosci.* **2**, 79–87 (1999).
6. K. Friston, A theory of cortical responses. *Philos. Trans. R. Soc. Lond. B Biol. Sci.* **360**, 815–836 (2005).
7. A. M. Bastos, W. M. Usrey, R. A. Adams, G. R. Mangun, P. Fries, K. J. Friston, Canonical microcircuits for predictive coding. *Neuron* **76**, 695–711 (2012).
8. P. A. Salin, J. Bullier, Corticocortical connections in the visual system: Structure and function. *Physiol. Rev.* **75**, 107–154 (1995).
9. V. A. Lamme, H. Supér, H. Spekreijse, Feedforward, horizontal, and feedback processing in the visual cortex. *Curr. Opin. Neurobiol.* **8**, 529–535 (1998).
10. N. T. Markov, M. Ersey-Ravasz, D. C. Van Essen, K. Knoblauch, Z. Toroczkai, H. Kennedy, Cortical high-density counterstream architectures. *Science* **342**, 1238406 (2013).
11. T. van Kerkoerle, M. W. Self, B. Dagnino, M.-A. Gariel-Mathis, J. Poort, C. van der Togt, P. R. Roelfsema, Alpha and gamma oscillations characterize feedback and feedforward processing in monkey visual cortex. *Proc. Natl. Acad. Sci. U.S.A.* **111**, 14332–14341 (2014).
12. A. M. Bastos, J. Vezoli, C. A. Bosman, J.-M. Schoffelen, R. Oostenveld, J. R. Dowdall, P. De Weerd, H. Kennedy, P. Fries, Visual areas exert feedforward and feedback influences through distinct frequency channels. *Neuron* **85**, 390–401 (2015).
13. P. Fries, Rhythms for cognition: Communication through coherence. *Neuron* **88**, 220–235 (2015).
14. G. Michalareas, J. Vezoli, S. van Pelt, J.-M. Schoffelen, H. Kennedy, P. Fries, Alpha-beta and gamma rhythms subserve feedback and feedforward influences among human visual cortical areas. *Neuron* **89**, 384–397 (2016).
15. S. Xie, D. Kaiser, R. M. Cichy, Visual imagery and perception share neural representations in the alpha frequency band. *Curr. Biol.* **30**, 2621–2627.e5 (2020).
16. D. Kaiser, Spectral brain signatures of aesthetic natural perception in the α and β frequency bands. *J. Neurophysiol.* **128**, 1501–1505 (2022).
17. J. D. Haynes, A primer on pattern-based approaches to fMRI: Principles, pitfalls, and perspectives. *Neuron* **87**, 257–270 (2015).
18. D. J. Mannion, D. J. Kersten, C. A. Olman, Regions of mid-level human visual cortex sensitive to the global coherence of local image patches. *J. Cogn. Neurosci.* **26**, 1764–1774 (2014).
19. D. Kaiser, R. M. Cichy, Parts and wholes in scene processing. *J. Cogn. Neurosci.* **34**, 4–15 (2021).
20. S. Clavagnier, A. Falchier, H. Kennedy, Long-distance feedback projections to area V1: Implications for multisensory integration, spatial awareness, and visual consciousness. *Cogn. Affect. Behav. Neurosci.* **4**, 117–126 (2004).
21. L. Muckli, L. S. Petro, Network interactions: Non-geniculate input to V1. *Curr. Opin. Neurobiol.* **23**, 195–201 (2013).
22. R. M. Cichy, D. Pantazis, A. Oliva, Resolving human object recognition in space and time. *Nat. Neurosci.* **17**, 455–462 (2014).
23. R. M. Cichy, A. Oliva, A M/EEG-fMRI fusion primer: Resolving human brain responses in space and time. *Neuron* **107**, 772–781 (2020).
24. C. I. P. Winlove, F. Milton, J. Ranson, J. Fulford, M. MacKisack, F. Macpherson, A. Zeman, The neural correlates of visual imagery: A co-ordinate-based meta-analysis. *Cortex* **105**, 4–25 (2018).

25. F. Ragni, A. Lingnau, L. Turella, Decoding category and familiarity information during visual imagery. *Neuroimage* **241**, 118428 (2021).
26. P. Vetter, F. W. Smith, L. Muckli, Decoding sound and imagery content in early visual cortex. *Curr. Biol.* **24**, 1256–1262 (2014).
27. P. Vetter, Ł. Bola, L. Reich, M. Bennett, L. Muckli, A. Amedi, Decoding natural sounds in early “visual” cortex of congenitally blind individuals. *Curr. Biol.* **30**, 3039–3044.e2 (2020).
28. F. W. Smith, L. Muckli, Nonstimulated early visual areas carry information about surrounding context. *Proc. Natl. Acad. Sci. U.S.A.* **107**, 20099–20103 (2010).
29. L. Muckli, F. De Martino, L. Vizioli, L. S. Petro, F. W. Smith, K. Ugurbil, R. Goebel, E. Yacoub, Contextual feedback to superficial layers of V1. *Curr. Biol.* **25**, 2690–2695 (2015).
30. A. J. Keller, M. M. Roth, M. Scanziani, Feedback generates a second receptive field in neurons of the visual cortex. *Nature* **582**, 545–549 (2020).
31. L. Kirchberger, S. Mukherjee, M. W. Self, P. R. Roelfsema, Contextual drive of neuronal responses in mouse V1 in the absence of feedforward input. *Sci. Adv.* **9**, eadd2498 (2023).
32. P. Papale, F. Wang, A. T. Morgan, X. Chen, A. Gilhuis, L. S. Petro, L. Muckli, P. R. Roelfsema, M. W. Self, Feedback brings scene information to the representation of occluded image regions in area V1 of monkeys and humans. *bioRxiv* 2022.11.21.517305 [Preprint]. 22 November 2022. <https://doi.org/10.1101/2022.11.21.517305>.
33. S. Dehaene, L. Cohen, Cultural recycling of cortical maps. *Neuron* **56**, 384–398 (2007).
34. M. A. Williams, C. I. Baker, H. P. Op de Beeck, W. Mok Shim, S. Dang, C. Triantafyllou, N. Kanwisher, Feedback of visual object information to foveal retinotopic cortex. *Nat. Neurosci.* **11**, 1439–1445 (2008).
35. M. Bilalić, L. Lindig, L. Turella, Parsing rooms: The role of the PPA and RSC in perceiving object relations and spatial layout. *Brain Struct. Funct.* **224**, 2505–2524 (2019).
36. D. Kaiser, G. Häberle, R. M. Cichy, Cortical sensitivity to natural scene structure. *Hum. Brain Mapp.* **41**, 1286–1295 (2020).
37. K. E. Stephan, J. C. Marshall, W. D. Penny, K. J. Friston, G. R. Fink, Interhemispheric integration of visual processing during task-driven lateralization. *J. Neurosci.* **27**, 3512–3522 (2007).
38. T. Mima, T. Oluwatimilehin, T. Hiraoka, M. Hallett, Transient interhemispheric neuronal synchrony correlates with object recognition. *J. Neurosci.* **21**, 3942–3948 (2001).
39. J. D. Watson, R. Myers, R. S. Frackowiak, J. V. Hajnal, R. P. Woods, J. C. Mazziotta, S. Shipp, S. Zeki, Area V5 of the human brain: Evidence from a combined study using positron emission tomography and magnetic resonance imaging. *Cereb. Cortex* **3**, 79–94 (1993).
40. R. B. Tootell, J. B. Reppas, K. K. Kwong, R. Malach, R. T. Born, T. J. Brady, B. R. Rosen, J. W. Belliveau, Functional analysis of human MT and related visual cortical areas using magnetic resonance imaging. *J. Neurosci.* **15**, 3215–3230 (1995).
41. D. Cohen, E. Goddard, K. T. Mullen, Reevaluating hMT+ and hV4 functional specialization for motion and static contrast using fMRI-guided repetitive transcranial magnetic stimulation. *J. Vis.* **19**, 11 (2019).
42. G. Pfurtscheller, A. Stancák, C. Neuper, Event-related synchronization (ERS) in the alpha band — an electrophysiological correlate of cortical idling: A review. *Int. J. Psychophysiol.* **24**, 39–46 (1996).
43. V. Romei, V. Brodbeck, C. Michel, A. Amedi, A. Pascual-Leone, G. Thut, Spontaneous fluctuations in posterior α -band EEG activity reflect variability in excitability of human visual areas. *Cereb. Cortex* **18**, 2010–2018 (2008).
44. O. Jensen, A. Mazaheri, Shaping functional architecture by oscillatory alpha activity: Gating by inhibition. *Front. Hum. Neurosci.* **4**, 186 (2010).
45. S. Haegens, V. Nächer, R. Luna, R. Romo, O. Jensen, α -Oscillations in the monkey sensorimotor network influence discrimination performance by rhythmical inhibition of neuronal spiking. *Proc. Natl. Acad. Sci. U.S.A.* **108**, 19377–19382 (2011).
46. M. S. Clayton, N. Yeung, R. Cohen Kadosh, The roles of cortical oscillations in sustained attention. *Trends Cogn. Sci.* **19**, 188–195 (2015).
47. D. Jokisch, O. Jensen, Modulation of gamma and alpha activity during a working memory task engaging the dorsal or ventral stream. *J. Neurosci.* **27**, 3244–3251 (2007).
48. I. E. J. de Vries, H. A. Slagter, C. N. L. Olivers, Oscillatory control over representational states in working memory. *Trends Cogn. Sci.* **24**, 150–162 (2020).
49. A. M. Bastos, M. Lundqvist, A. S. Waite, N. Kopell, E. K. Miller, Layer and rhythm specificity for predictive routing. *Proc. Natl. Acad. Sci. U.S.A.* **117**, 31459–31469 (2020).
50. M. S. Clayton, N. Yeung, R. Cohen Kadosh, The many characters of visual alpha oscillations. *Eur. J. Neurosci.* **48**, 2498–2508 (2018).
51. A. Clark, Whatever next? Predictive brains, situated agents, and the future of cognitive science. *Behav. Brain Sci.* **36**, 181–204 (2013).
52. Y. Hu, Q. Yu, Spatiotemporal dynamics of self-generated imagery reveal a reverse cortical hierarchy from cue-induced imagery. *bioRxiv* 2023.01.25.525474 [Preprint]. 25 January 2023. <https://doi.org/10.1101/2023.01.25.525474>.
53. A. Alamia, R. VanRullen, Alpha oscillations and traveling waves: Signatures of predictive coding? *PLOS Biol.* **17**, e3000487 (2019).
54. D. Lozano-Soldevilla, R. VanRullen, The hidden spatial dimension of alpha: 10-Hz perceptual echoes propagate as periodic traveling waves in the human brain. *Cell Rep.* **26**, 374–380.e4 (2019).
55. G. Kreiman, T. Serre, Beyond the feedforward sweep: Feedback computations in the visual cortex. *Ann. N. Y. Acad. Sci.* **1464**, 222–241 (2020).
56. G. W. Lindsay, Convolutional neural networks as a model of the visual system: Past, present, and future. *J. Cogn. Neurosci.* **33**, 2017–2031 (2021).
57. D. H. Brainard, The psychophysics toolbox. *Spat. Vis.* **10**, 433–436 (1997).
58. D. G. Pelli, The VideoToolbox software for visual psychophysics: Transforming numbers into movies. *Spat. Vis.* **10**, 437–442 (1997).
59. H. E. M. den Ouden, J. Daunizeau, J. Roiser, K. J. Friston, K. E. Stephan, Striatal prediction error modulates cortical coupling. *J. Neurosci.* **30**, 3210–3219 (2010).
60. R. Oostenveld, P. Fries, E. Maris, J.-M. Schoffelen, FieldTrip: Open source software for advanced analysis of MEG, EEG, and invasive electrophysiological data. *Comput. Intell. Neurosci.* **2011**, 156869 (2011).
61. N. N. Oosterhof, A. C. Connolly, J. V. Haxby, CoSMoMVPA: Multi-modal multivariate pattern analysis of neuroimaging data in Matlab/GNU Octave. *Front. Neuroinform.* **10**, 27 (2016).
62. C.-C. Chang, C.-J. Lin, LIBSVM. *ACM Trans. Intell. Syst. Technol.* **2**, 1–27 (2011).
63. L. Chen, R. M. Cichy, D. Kaiser, Semantic scene-object consistency modulates N300/400 EEG components, but does not automatically facilitate object representations. *Cereb. Cortex* **32**, 3553–3567 (2022).
64. C. Hutton, A. Bork, O. Josephs, R. Deichmann, J. Ashburner, R. Turner, Image distortion correction in fMRI: A quantitative evaluation. *Neuroimage* **16**, 217–240 (2002).
65. J. S. Prince, I. Charest, J. W. Kurzwski, J. A. Pyles, M. J. Tarr, K. N. Kay, Improving the accuracy of single-trial fMRI response estimates using GLMsingle. *eLife* **11**, e77599 (2022).
66. K. Grill-Spector, The neural basis of object perception. *Curr. Opin. Neurobiol.* **13**, 159–166 (2003).
67. D. D. Dilks, J. B. Julian, A. M. Paunov, N. Kanwisher, The occipital place area is causally and selectively involved in scene perception. *J. Neurosci.* **33**, 1331–1336 (2013).
68. E. Maguire, The retrosplenial contribution to human navigation: A review of lesion and neuroimaging findings. *Scand. J. Psychol.* **42**, 225–238 (2001).
69. R. A. Epstein, C. I. Baker, Scene Perception in the Human Brain. *Annu. Rev. Vis. Sci.* **5**, 373–397 (2019).
70. R. Epstein, A. Harris, D. Stanley, N. Kanwisher, The parahippocampal place area. *Neuron* **23**, 115–125 (1999).
71. J. B. Julian, E. Fedorenko, J. Webster, N. Kanwisher, An algorithmic method for functionally defining regions of interest in the ventral visual pathway. *Neuroimage* **60**, 2357–2364 (2012).
72. M. Rosenke, R. van Hoof, J. van den Hurk, K. Grill-Spector, R. Goebel, A probabilistic functional atlas of human occipito-temporal visual cortex. *Cereb. Cortex* **31**, 603–619 (2021).

Acknowledgments: We thank D. Marinova and A. Carter for help in EEG data acquisition. We would also thank the HPC Service of ZEDAT, Freie Universität Berlin, for computing time.

Funding: L.C. is supported by a PhD stipend from the China Scholarship Council (CSC). R.M.C. is supported by the Deutsche Forschungsgemeinschaft (DFG; CI241/1-1, CI241/3-1, and CI241/7-1) and by a European Research Council (ERC) starting grant (ERC-2018-STG 803370). D.K. is supported by the DFG (SFB/TRR135 – INST162/567-1, project number 222641018), an ERC starting grant (PEP, ERC-2022-STG 101076057), and “The Adaptive Mind” funded by the Excellence Program of the Hessian Ministry of Higher Education, Science, Research and Art. Views and opinions expressed are those of the authors only and do not necessarily reflect those of the European Union or the European Research Council. Neither the European Union nor the granting authority can be held responsible for them. **Author contributions:** Conceptualization: L.C. and D.K. Methodology: L.C. and D.K. Software: L.C. and D.K. Formal analysis: L.C. Investigation: L.C. and D.K. Resources: L.C. and D.K. Data curation: L.C. Writing—original draft: L.C. and D.K. Writing—review and editing: L.C., R.M.C., and D.K. Visualization: L.C. Supervision: R.M.C. and D.K. Project administration: R.M.C. and D.K. Funding acquisition: R.M.C. and D.K. **Competing interests:** The authors declare that they have no competing interests. **Data and materials availability:** All data needed to evaluate the conclusions in the paper are present in the paper and/or the Supplementary Materials. Raw data used in the analyses are available at the following Zenodo repository: <https://doi.org/10.5281/zenodo.8369131>. Processed data and code used in the analyses are available at the following Zenodo repository: <https://doi.org/10.5281/zenodo.8369136>.

Submitted 12 April 2023

Accepted 12 October 2023

Published 10 November 2023

10.1126/sciadv.adi2321

Alpha-frequency feedback to early visual cortex orchestrates coherent naturalistic vision

Lixiang Chen, Radoslaw M. Cichy, and Daniel Kaiser

Sci. Adv. **9** (45), eadi2321. DOI: 10.1126/sciadv.adi2321

View the article online

<https://www.science.org/doi/10.1126/sciadv.adi2321>

Permissions

<https://www.science.org/help/reprints-and-permissions>

Use of this article is subject to the [Terms of service](#)

Science Advances (ISSN 2375-2548) is published by the American Association for the Advancement of Science. 1200 New York Avenue NW, Washington, DC 20005. The title *Science Advances* is a registered trademark of AAAS.

Copyright © 2023 The Authors, some rights reserved; exclusive licensee American Association for the Advancement of Science. No claim to original U.S. Government Works. Distributed under a Creative Commons Attribution NonCommercial License 4.0 (CC BY-NC).